Selective inhibition of excitatory synaptic transmission alters the emergent bursting dynamics of in vitro neural networks

Janelle Shari Weir[1]*, Nicholas Christiansen[1], Axel Sandvig[1,2,3], Ioanna Sandvig[1]

[1]Department of Neuromedicine and Movement Science, Faculty of Medicine and Health Sciences, Norwegian University of Science and Technology (NTNU), Trondheim, Norway

[2]Department of Pharmacology and Clinical Neurosciences, Division of Neuro, Head and Neck, Umeå University Hospital, Umeå, Sweden

[3] Department of Community Medicine and Rehabilitation, Division of Neuro, Head and Neck, Umeå University Hospital, Umeå, Sweden

*** Correspondence:**
janelle.s.weir@ntnu.no

Keywords: Cortical network; excitatory-inhibitory balance; network activity; network bursts; chemogenetics; electrophysiology; DREADDs

Abstract *(<250 words)*

Neurons in vitro connect to each other and form neural networks that display emergent electrophysiological activity. This activity begins as spontaneous uncorrelated firing in the early phase of development, and as functional excitatory and inhibitory synapses mature, this activity typically emerges as spontaneous network bursts. Network bursts are events of coordinated global activation among many neurons interspersed with periods of silencing and are important for synaptic plasticity, neural information processing, and network computation. While bursting is the consequence of balanced excitatory-inhibitory (E/I) interactions, the functional mechanisms underlying their evolution from physiological to potentially pathophysiological states are still poorly understood. This is partly because we have limited knowledge of and access to the synaptic connections themselves. In this study, we used selective chemogenetic inhibition to target and disrupt excitatory synaptic transmission in in vitro neural networks to study functional response and recovery of spontaneous network bursts over time. We found that inhibition resulted in neural networks subsequently exhibiting high frequency network bursts with high number of spikes per bursts, and with up to 98% of all spikes being in network bursts. Our results imply that the disruption in excitatory synaptic transmission during early network development likely affected inhibitory synaptic maturity which resulted in an overall decrease in network inhibition at later stages. These findings give evidence to the importance of E/I balance in maintaining physiological bursting patterns in neural networks.

1 Introduction

Neural network dynamics emerge over the course of development in vitro. Spontaneous network activity starts as immature tonic spiking in the early phases between 3 –5 days in vitro (DIV), and then progresses towards more complex behaviour characterized by bursts (Fardet et al., 2018). Typically, in vitro neural networks start exhibiting bursts between 6 and 14 DIV (Chiappalone et al., 2006, Wagenaar et al., 2006). Such early bursts, described as "superbursts" (Stephens et al., 2012), are posited to be driven by depolarizing gamma – aminobutyric acid type A ($GABA_A$) receptors and are hallmarks of early network development. At this stage, neuronal interactions are strengthened leading to recurrent coactivation among several neurons, which manifest as network bursts. These network bursts become more recurring as the neural network reaches maturity around 21 DIV and onwards, with burst profile of higher frequency, shorter burst onset and offset, and shorter duration (Chiappalone et al., 2006, Bisio et al., 2014).

Network bursts are shown to be driven by excitatory synaptic transmission (Robinson et al., 1993, Kudela et al., 2003, Teppola et al., 2019), primarily mediated by glutamatergic ionotropic N-methyl-D-aspartate (NMDA) receptors and alpha-amino-3-hydroxy-5-methyl-4-isoxazolepropionic acid (AMPA) receptors. Fast inhibition by $GABA_A$ receptors also mediates network activity and burst emergence by maintaining a balance in excitatory – inhibitory (E/I) synaptic transmission (Teppola et al., 2019). Early in vitro studies reported that the relationship between network age, structure and the resulting activity is due to variations in synaptic connections and the differential developmental periods of excitatory and inhibitory synaptic transmission (Burgard and Hablitz, 1994, Kamioka et al., 1996). As the network achieves adequate interconnectivity and inhibitory synapses become more functionally mature during the later stages of development, network dynamics are reported to progress from spontaneous uncorrelated firing to more complex patterns of synchronized network bursts (Kamioka et al., 1996, Opitz et al., 2002, Wagenaar et al., 2006, Baltz et al., 2010). These important in vitro observations mirror closely in vivo network development. Several in vivo studies have reported similar age specific correlation of the emergence of network bursts with functional circuit development in various parts of the nervous system including the hippocampus (Blankenship and Feller, 2010, Raus Balind et al., 2019), cerebellar cortex (Dizon and Khodakhah, 2011, Hoehne et al., 2020), visual cortex (Chiu and Weliky, 2001), medulla (Pena and Ramirez, 2004, Magalhaes et al., 2021) and spinal cord (Darbon et al., 2004). These findings suggest that excitatory and inhibitory synaptic maturity are important drivers of network bursts, burst characteristics and subsequent network function. The effect of selective disruption of E/I balance on bursting dynamics in neural networks may therefore reveal substantial biological insights into network function, adaptability, and robustness.

Investigating inhibitory – excitatory synaptic contribution to network burst evolution in vivo is challenging. This is in part because the brain comprises numerous complex multi-layered neural networks, with heterogeneous synaptic connectivity among subsets of burst-generating neurons that contribute to the dynamics of the network (Zeldenrust et al., 2018). The interweaving of different neurons and synapses at various topological and temporal scales makes it a challenge to determine the relative impact of synaptic activity on physiological and pathophysiological bursting activity. Since in vitro neural networks represent a monolayered reductionist model of a brain network – while still

maintaining salient age dependent electrophysiological dynamics (Ben-Ari, 2001, Chiappalone et al., 2006, Chiappalone et al., 2007, Sun et al., 2010, Schroeter et al., 2015) – the complexity is reduced along spatial dimensions, and thus enables study and selective manipulation in a controlled manner (Marom and Shahaf, 2002). Many studies have taken advantage of such reductionist in vitro models to investigate network burst dynamics at the synaptic level via manipulation that changes the balance between excitatory and inhibitory synaptic transmission. Methods such as pharmacological blockade of NMDA and AMPA receptors (Chub and O'Donovan, 1998, Li et al., 2007, Suresh et al., 2016) and membrane current blockers (Ramakers et al., 1990, Ramakers et al., 1994, van Drongelen et al., 2006) have provided significant insights into the functional contribution of synaptic receptors and intrinsic membrane currents to the generation, maintenance, duration, and propagation of network bursts. In this study, we utilized hM4Di designer receptors exclusively activated by designer drugs (DREADDs) (Armbruster et al., 2007, Alexander et al., 2009, Urban and Roth, 2015, Khambhati and Bassett, 2016, Whissell et al., 2016, Panthi and Leitch, 2019, Haaranen et al., 2020a, Haaranen et al., 2020b, Lebonville et al., 2020, Ozawa and Arakawa, 2021) to selectively inhibit excitatory synaptic transmission – via G-protein coupled receptors (GPCRs) in calcium/calmodulin-dependent protein kinase alpha (CaMKlla) expressing neurons – in neural networks interfaced with microelectrode arrays (MEAs). Networks were chemogenetically inhibited at 14 DIV, 21 DIV and 28 DIV and their dynamics characterized in comparison to baseline activity and to control, unperturbed networks. The internal characteristics of both network bursts during treatment (functional response to perturbation) and post treatment (recovery of the network) were analyzed. We found that inhibition of excitatory inputs caused sustained high burst frequency within neural networks, as well as increased network synchronization. Our results suggest a decrease in overall network inhibition, and that the long-term maintenance of the E/I excitatory – inhibitory balance depends on ongoing excitatory synaptic activity.

2 Materials and Methods

2.1 Culture of cortical networks on microelectrode arrays

Primary rat (Sprague Dawley) cortex neurons were obtained from ThermoFisher Scientific, US (Cat. No: A36511). Cells were thawed and seeded as a co-culture with 15% rat primary cortical astrocytes also from ThermoFisher Scientific (Cat. No: N7745100). The cells were plated at a density of approximately 1000 cells/mm^2 on Nunc™ Lab -Tek™ Chamber Slides coated with Geltrex matrix (cat. No. A1413201) at a working concentration of 0.5ug/cm^2 for 1:100 dilution. Both obtained from ThermoFisher Scientific. Pre-sterilized 6-well CytoView MEA plates were purchased from Axion Biosystems and coated with 0.5% polyethyleneimine diluted in HEPES (both from Sigma-Aldrich) and 20 µg/mL natural mouse laminin (ThermoFisher Scientific) diluted in DPBS according to the Axion coating protocol (Axion BioSystems, Georgia, USA). Cells were plated directly over the electrodes on Axion MEA plates at a density of approximately 1500 cells/mm^2 and incubator for 4hrs before topping up wells to 1mL with media. Cells were plated and maintained in Neurobasal™ Plus Medium supplemented with 2% B-27 Plus Supplement and 0.5% GlutaMAX™ all from ThermoFisher Scientific. The culture media was also supplemented with 0.2% (1:500 dilution from a 5 µg/ml working concentration) Plasmocin™ Prophylactic (ant. mpp; InvivoGen). The day of plating

from cryopreservation was allocated as day 0 and 50% media changes were carried out every 2-3 days. Cells were always kept in a 5%CO_2 incubator at 37ºC except during media changes and imaging.

2.2 AAV 2/1 hM4Di CaMKlla-DREADDs production and in vitro transduction

Vector production and purification was performed in-house at the Viral Vector Core Facility (Kavli Institute, NTNU). Tittering of the viral stock was determined as approximately 10^{11} vg/mL. High viral stocks were aliquoted into 20ul volumes and stored at -80 ºC. Aliquots for use were thawed on ice and remaining virus aliquoted at store at -80ºC. The maximum number of thaws for any aliquot used was 3 times. At 7 DIV, the neurons were transduced by removing 80% of the cell media from the culture and directly adding a dilution of AAV viral particles encoding experimental hM4Di -CaMKlla-DREADDs to the neurons (**Figure 1A**). The titer of the viral dilution used for each well was 1 x 10^3 viral units per neuron based on tests at different viral concentrations (results not included). The cultures were gently agitated for 30 seconds to ensure proper distribution of the viral particles and then incubated for 8hrs. Afterwards, each well was topped up to 1mL with fresh media without Plasmocin™ Prophylactic and incubated for an additional 40hrs in 5%CO_2, 37ºC incubator. After the incubation period, 50% media changes were carried out as scheduled. The vector encodes mCherry which is a bright red fluorescent protein tag that makes it possible to visualize results soon after transduction (**Figure 1B**).

2.3 Immunocytochemistry

At 14 DIV, parallel hM4Di DREADD networks were immunolabeled to investigate the specificity for vector mediated hM4Di expression in the CaMKlla positive neurons. The cultures were fixed with 4% Paraformaldehyde (PFA) for 20 minutes and washed with DPBS before cultures were permeabilized with a blocking solution of 0.03% Triton X-100 and 5% goat serum in DPBS for 2 hours at room temperature. Following blocking, antibodies at the indicated solutions **(Table 1)** were added in a buffer of 0.01% Triton X-100 and 1% goat serum in DPBS. Nuclei were stained with Hoechst (bisbenzimide H 33342 trihydrochloride, 14533, Sigma-Aldrich, 1: 5000 dilution). Samples were washed, mounted on glass cover slides with anti-fade fluorescence mounting medium (ab104135, Abcam) and imaged. All sample images were acquired using the EVOS M5000 imaging system (Invitrogen ThermoFisher Scientific). Images were processed using Fiji/ImageJ and Adobe Illustrator 2020 version: 24.0.0.

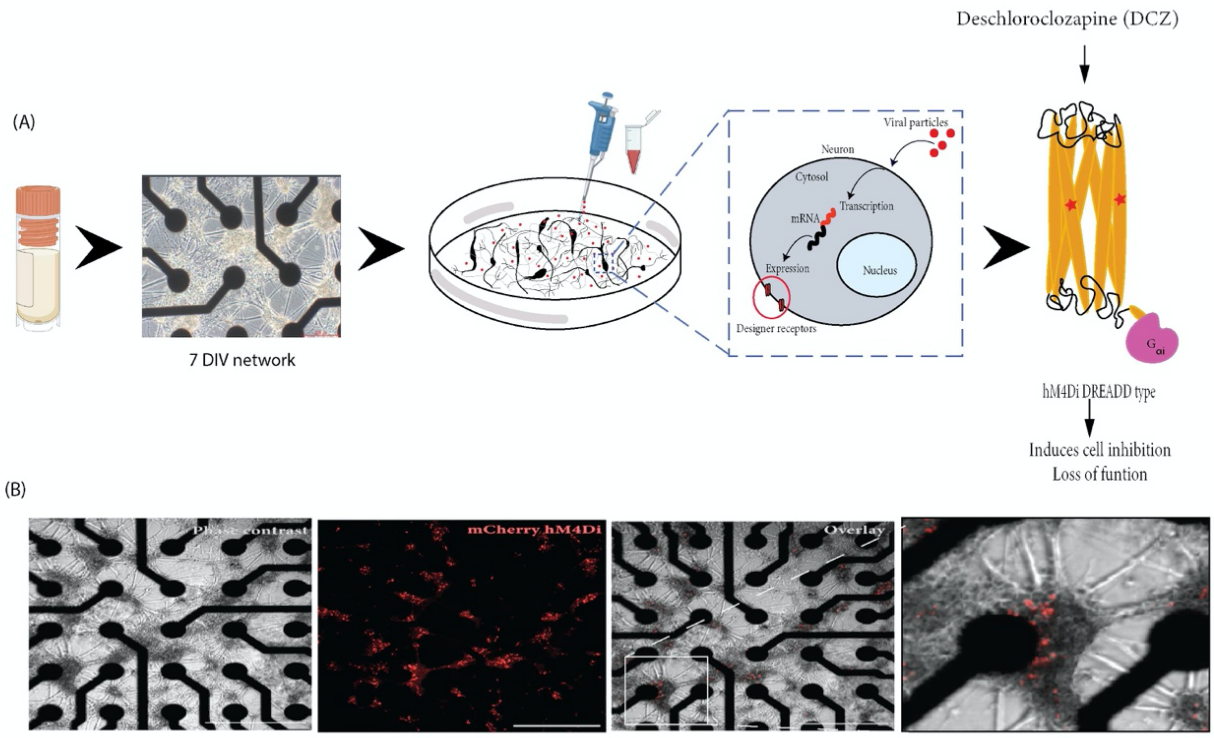

Figure 1. Illustration of the workflow of the study. **(A)** Cryopreserved cortical neurons were thawed and seeded on precoated MEAs until 7 DIV (scale bar = 200 µm). Neurons grow on top of the electrodes (black) and connect with each other across the surface. The DREADD protein is encoded in a replication deficient adeno-associated viral vector (AAV2/1) that is targeted for cytoplasmic gene delivery, thus circumventing genomic integration. The vector was added directly to the neurons in culture (on the MEA). The vector codes for the cell-specific promoter CaMKll so that mRNA transcription is targeted specifically at excitatory neurons which will be the cells that express the designer receptors. The designed DREADD hM4Di receptor has mutations at two points, which results in the receptor being insensitive to its endogenous agonist and neurotransmitter acetylcholine and instead respond only to a physiologically inert exogenous molecule (designer drug) such as deschloroclozapine (DCZ). When DCZ binds, the hM4DiR preferentially signals through the Gai/o subset of G-protein to inhibit adenylate cyclase and downstream cyclic adenosine monophosphate (cAMP) production, causing neuronal hyperpolarization and induces loss of cellular activity. **(B)** In vitro neural network on MEA at 12 days post adding the virus. DREADDs expression was confirmed without immunocytochemistry based on strong mCherry fluorescent expression in the network. Scale bar = 1250µm

137 **Table 1.** Overview of primary and secondary antibodies, species, and concentrations.

138

Primaries			Secondaries		
Markers	**Catalogue #**	**Concentration**	**Fluorescent**	**Catalogue #**	**Concentration**
Ck mCherry	Ab205402	1:1000	Goat-anti-Chicken AlexaFluor 568	Ab175477	1:1000
Ms Calmodulin (CaMKll)	MA3-918	1:250	Goat-anti-Mouse AlexaFluor 568	A11019	1:1000
Ms NMDAR1	32-0500	1:100	Goat-anti-Mouse AlexaFluor 647	A21236	1:1000
Ms GABA BR1	Ab55051	1:250	Goat-anti-Mouse AlexaFluor 488	A11001	1:1000
Rb Calmodulin (CaMKll)	Ab134041	1:200	Goat-anti-Rabbit AlexaFluor 568	A11011	1:1000
Rb Glutamate decarboxylase (GAD65/67)	Ab183999	1:100	Goat-anti-Rabbit AlexaFluor 647	A21244	1:1000
Rb Map2	Ab32454	1:250	Goat-anti-Rabbit AlexaFluor 488	A11008	1:1000
Rb Glial fibrillary acidic protein (GFAP)	Ab278054	1:500			

139

140 ## 2.4 Extracellular electrophysiological recordings

141 Neural activity was recorded on the Axion Maestro Pro MEA system (Axion BioSystems, Georgia, USA) with an
142 integrated temperature-controlled CO_2 incubator (temperature 37^0C and 5% CO_2). Data acquisition was done through
143 the AxIS Navigator Software version 3.1.1. Spontaneous neuronal activity was recorded across 4 weeks (at 14, 21,
144 28 and 35 DIV). Spiking data was captured using the AxIS spike detector with an Adaptive threshold crossing. Spikes
145 were defined by a threshold of 7 standard deviations of the internal noise level with a post/pre-spike duration of
146 2.16/2.84 ms of each individual electrode, and with frequency limits of 200Hz – 3kHz. Spike sorting was not
147 attempted.

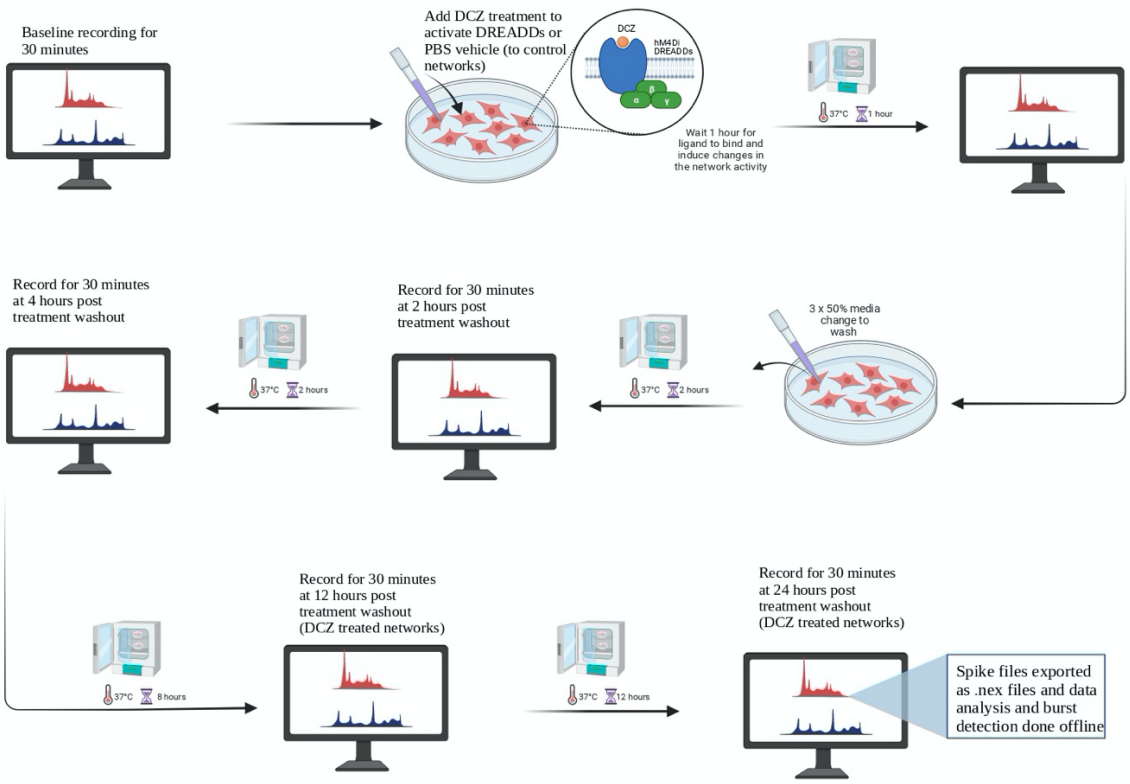

Figure 2. Recording workflow with treatment and wash out. Created with BioRender.com

2.5 Chemogenetic manipulation

To investigate the network response to chemogenetic manipulation, the novel synthetic ligand DCZ (MedChemExpress) was used to activate the DREADDs receptors (Nagai et al., 2020, Bjorkli et al., 2022) to induce synaptic silencing in excitatory neurons (see **Figure 2** for workflow). In summary, MEA plates were incubated for 15 minutes in the Maestro Pro chamber before recording baseline spontaneous network activity. Afterwards, either PBS (vehicle) or DCZ diluted in PBS (treatment) was added to 45% media volume in the wells at a final DCZ concentration of 10 µM. Networks were incubated for 1 hour and then recorded for 1hr. Thereafter, 3 x 50% media changes were performed to wash out DCZ in the inhibited networks, and 1 x 50% media change done in the PBS treated networks. Networks were recorded after washout (see **Table 2** for overview of networks recordings and analysis done). Of the inhibited networks, a total of 6 networks were studied, 3 were excluded from analysis due to these networks exhibiting mean firing rate < 0.01 spikes/s at a

threshold of 7 x standard deviation. Of the PBS treated networks, 2 were studied and both analyzed. For the control networks (no DREADDs – no DCZ – no PBS), 2 were studied and 1 network was excluded from the analysis due to the network exhibiting mean firing rate < 0.01 spikes/s at a threshold of 7 x standard deviation. Each network was analyzed independently.

Table 2. Overview of networks analyzed, conditions, treatments received, and recordings done.

Neuronal networks analyzed	Conditions	Protocol	Electrophysiology recording
Control x 1 network	No DREADDs, No DCZ treatment, No PBS vehicle	-	Baseline
Control x 2 networks	DREADDs + PBS vehicle	50ul PBS added to 450ul media	Baseline During PBS vehicle Recovery at 2hrs Recovery at 4hrs
Treatment x 3 networks	DREADDs + DCZ treatment	5ul (from 1mM stock) DCZ diluted in 45ul PBS added to 450ul media	Baseline During DCZ treatment Recovery at 2hrs Recovery at 4hrs Recovery at 12hrs Recovery at 24hrs

2.6 Network dynamic analysis and network bursts detection

The recording spike frequency was computed using the equation: $f = \frac{(spikes-1)}{\Delta t}$,

where spikes are the total number of spikes for a recording channel and Δt is the time difference between the first and last spike included in spikes.

For shorter windows we define the spike frequency of the window as f_{window} as $f_{window} = \frac{spikes}{\Delta t}$,

where spikes are the spikes in the given window, and Δt is the width of the window of interest. The spike frequency was computed using a moving window of 1 second with a step size of 0.1 second, resulting in an overlap of windows for instantaneous measures.

Bursts were defined as sequences of at least four spikes with an interspike interval (ISI) lower than a threshold of 100ms for all electrodes. Network bursts were defined similarly as a sequence of spikes within a short temporal range on the cumulative spike train over all electrodes. The thresholds were detected automatically according to (Bakkum et al., 2013). An inter spike interval distribution between every six spikes was used to detect the peaks. Additionally, upper, and lower bounds were defined such that the threshold was bounded to a range of 12ms to 300ms as per (Gandolfo et al., 2010) (Obien et al., 2015). Burst analysis was performed to identify the number of spikes in each network burst (spikes in network burst) and the count of the number of network bursts generated with the number of

spikes (number of occurrence). Comparison between recording groups were assessed by Conover test with Bonferroni corrections for multiple comparisons.

3 Results

3.1 AAV2/1 Gi-DREADD is expressed exclusively in CaMKIIa positive neurons

AAV mediated-DREADDs expression was confirmed with immunolabeling to amplify mCherry expression in target CaMKIIa positive neurons (**Figure 3A**). Neither inhibitory neurons (GAD65/67) (**Figure 3B**), nor astrocytes (GFAP) (**Figure 3C**) showed co-labelling with mCherry. This confirmed that there was cell specific expression of the AAV-DREADDs. Furthermore, networks at 14 DIV positively expressed GABA (**Figure 4A**), GABA B receptors (**Figure 4B**) and NMDA receptors (**Figure 4C**) confirming network capacity for excitatory and inhibitory signaling at this age.

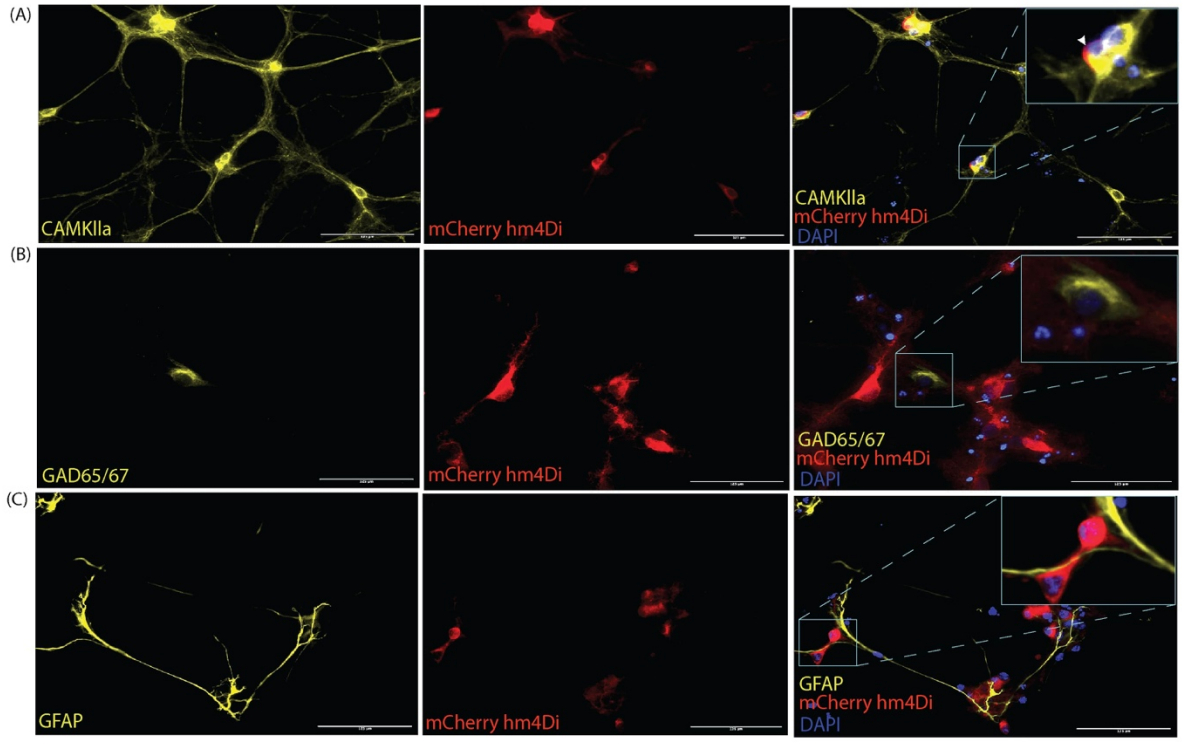

Figure 3. AAV2/1 hM4Di DREADDs expression in neurons in vitro. **(A)** The mCherry antibody was used to enhance the fluorescent of the hM4Di receptors, which were positively colocalized with the somata of CaMKIIa positive neurons. **(B)** GAD65/67 expression indicated the presence of inhibitory neurons and showed no soma colocalization mCherry hM4Di expression. **(C)** GFAP antibody was used to label astrocytes in the culture which also showed no soma colocalization with mCherry hM4Di expression. Scale bar = 125µm.

3.2 Spontaneous activity and burst characteristics at baseline

Spontaneous baseline activity captured at 14, 21 and 28 DIV revealed highly variable network activity as indicated by the distribution range of the mean firing rates in the box plot (**Figure 5A**). This variability was noticed across all networks. While the median values were similar within group, they were different between groups at 14 DIV, with PBS treated networks having the lowest overall median mean firing rate with most of the data points skewed higher

than the median. By 28 DIV, all groups had similar mean firing rates irrespective of manipulation. Interestingly, the control network and both PBS treated networks appeared to follow a similar development trend with mean firing rates increasing from between 0.01 and 0.03 Hz at 14 DIV, to between 0.1 and 0.2 Hz at 28 DIV (**Figure 5B)**. The inhibited networks had a more drastic increase from between 0.1 and 0.2 Hz at 14 DIV to between 0.6 and 0.9 Hz at 28 DIV. Network bursts were also present by 14 DIV with high variability in burst duration across the networks (**Figure 5C**). By 28 DIV, the network bursts in all inhibited networks occurred with shorter durations compared to recordings at 14 and 21 DIV and compared to control and PBS treated networks. An investigation into the characteristic of network bursts for all groups at 14 DIV (before any manipulation), revealed that spikes in network bursts followed a power law distribution. All networks exhibited most network bursts with between 4 to 10 spikes per burst occurrence (**Figure 5D-F**). The number of occurrences varied across networks, but only inhibited networks exhibited > 20 occurrences of bursts with <10 spikes. One inhibited network exhibited as many as 150 occurrences of bursts with < 10 spikes. Unsurprisingly, some network bursts containing over 100 spikes were identified for the inhibited networks, however, such bursts were not as frequent as those containing lower number of spikes. The ISI of neural activity in bursts also differed across the networks with the mean maximum ISI at 14 DIV being 1.3 milliseconds, and the minimum 0.07 milliseconds. Networks with bursts of longer ISIs (1.2 and 1.3 milliseconds) also had overall less occurrences of bursts than networks with shorter ISIs.

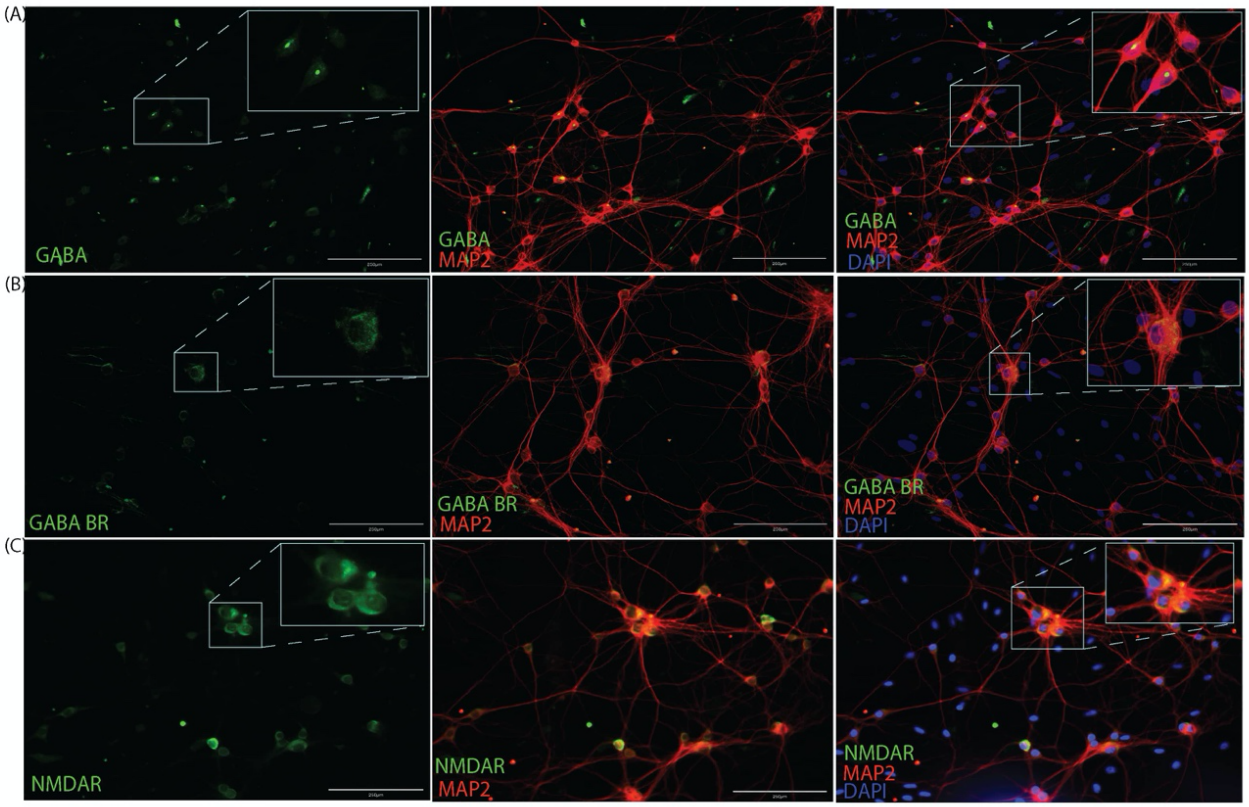

Figure 4. Immunocytochemistry for GABA **(A)**, GABAB receptors **(B)** and NMDA receptors **(C)** along with MAP2 neuronal cytoskeletal marker at 14 DIV. Scale bar 200 µm.

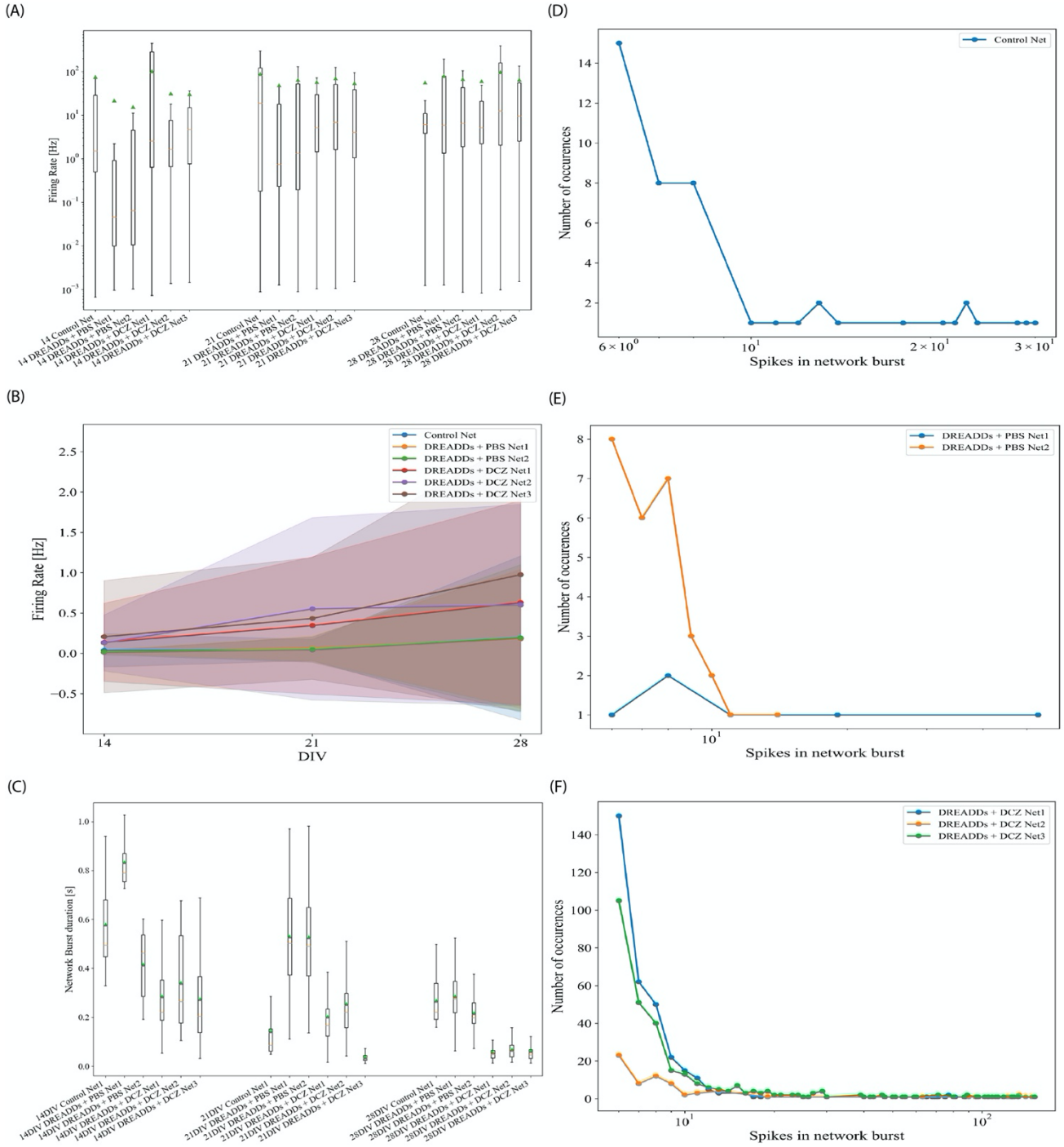

Figure 5. Mean firing rate and network burst composition at baseline. **(A)** Box plot depicting the spread of the distribution of the baseline mean firing rate (Hz) for Control, PBS vehicle and DCZ treatment networks at 14, 21 and 28 DIV. **(B)** The mean firing rate and mean ± standard deviation of the mean depicted by the lines and shaded regions respectively at 14, 21 and 28 DIV for all networks. **(C)** Box plot depicting the spread of the distribution of the network burst duration in seconds for all networks at 14, 21 and 28 DIV. Line graph showing the number of spikes in network bursts and the number of burst occurrences at 14DIV for Control network **(D)** PBS vehicle network **(E)** and DCZ treatment network **(F)**.

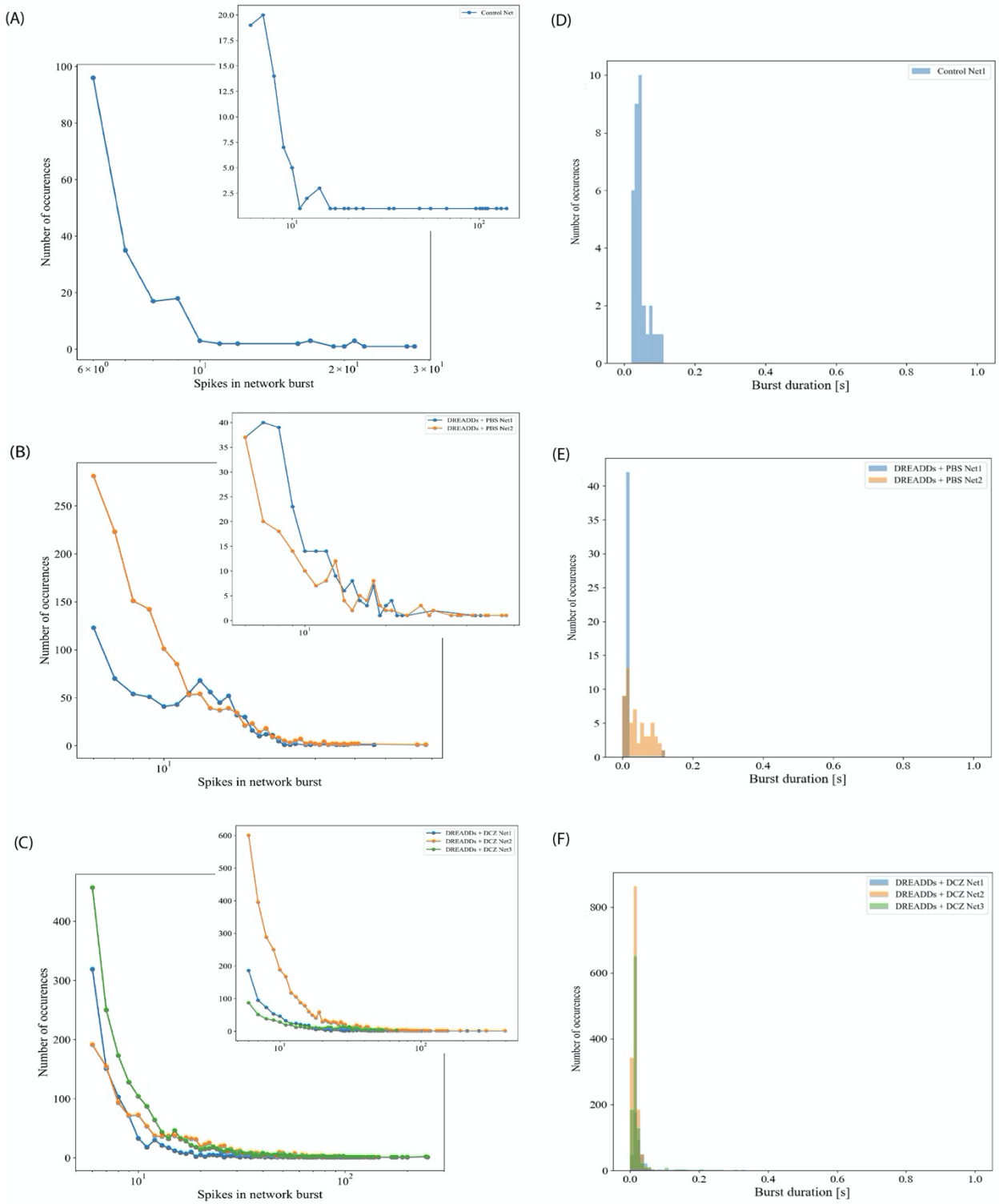

Figure 6. Network burst characteristics at 21 and 28 DIV and burst duration at 28 DIV. **(A-C upper right hand)** depict burst at 21 DIV. **(A-C lower left hand)** depict burst at 28 DIV. The x-axis denotes the number of spikes in network burst and the y-axis denotes the number of occurrences of burst of given number of spikes (ISI6-norm scale). **(D-F)** show for all networks the duration of bursts in seconds (x-axis), and the number of occurrences of bursts (y-axis).

3.3 Network burst composition and duration at 21 and 28 DIV across all networks

Due to the unique development of each network, and inherent variability between how network activity evolved, when making comparisons after 14 DIV, we looked at the overall trends in activity profile rather than directly comparing network dynamics between chemo-genetically perturbed and control or PBS treated networks. An unexpected finding was that there was a dramatic increase in bursting activity for the chemo-genetically perturbed networks which was sustained for the lifetime of the network. This influenced any direct comparison with control and PBS treated network activity development, thus comparison for differences in activity trends was more reliable.

Spontaneous network activity of the control and PBS treated networks followed a typical trajectory of development between 14 DIV and 28 DIV with increasingly more bursts as the networks reached maturity, according to previous work (Kamioka et al., 1996, Wagenaar et al., 2006). Similar to burst characteristics at 14 DIV, at 21 DIV (**Figure 6 A-C upper right-hand graphs)** most burst occurrences had <= 10 spikes, and fewer bursts had > 10 spikes. This was also true for all networks at 28 DIV (**Figure 6 A-C lower left-hand graphs**). Interestingly, the inhibited networks at both 21 and 28 DIV had overall more occurrences of bursts with < 10 spikes (up to 600 occurrences) than control and PBS treated networks. Inhibited networks also exhibited more bursts with > 10 spikes, including some network bursts with > 100 spikes per burst.

The inhibited networks also exhibited overall short mean ISIs of between 0.02 and 0.04 milliseconds at 21 DIV, which decreased to between 0.01 and 0.02 milliseconds by 28 DIV, indicating that spikes occurred closer together and that the networks had increased synchronization. Increased network synchronization was further supported by the shorter timeframe burst durations shown in inhibited networks compared to the control and PBS treated networks (**Figure 6D-F**). The control network showed mean burst duration at 0.1 seconds (**Figure 6D**), the PBS treated networks had mean burst duration between 0.1 and 0.3 seconds (**Figure 6E**), while inhibited networks had burst duration between 0.01 and 0.02 seconds (**Figure 6F**). Shorter bursts had the highest number of occurrences for all networks. Following the same trend as described previously for the number of spikes in network bursts, DCZ treated networks at 28 DIV had overall more occurrences of bursts with shorter duration (up to 800 occurrences) than control and PBS treated networks (between 10 and 40 occurrences).

3.4 Analysis of 28 DIV network response and network recovery due to selective inhibition

To identify the changes in activity in neural networks, we compared spontaneous baseline activities with activities during either DCZ treatment or PBS vehicle, as well as the network activities after DCZ removal at different time intervals. Chemo-genetically perturbed activity was analyzed in 3 phases of 20 minutes recordings – 1st phase, 2nd phase, and 3rd phase – to better characterize dynamic changes and response of the network. The baseline activity and inhibited activity are shown as the recording trace generated from 64 channels on the MEA (**Figure 7**). Prior to DCZ application, the spontaneous firing rate at baseline was stable for the entirety of the recording, observed as regular spikes with stable bursts (**Figure 7A**). As expected, the application of DCZ caused a decrease in network activity and ablation of networks bursts, which was captured during the 1st phase of recording (**Figure 7B**). The network started

exhibiting intermittent spikes and isolated bursts that gradually increased as the recording progressed (**Figure 7B-D**), indicating that network activity recovered in the presence of DCZ. We also noticed that while bursts were single occurrences with increasingly more spikes during DCZ 1st phase recording (**Figure 7E**), there was an increase in both the number of burst occurrences and spikes in network bursts at 2nd and 3rd phase recordings (**Figure 7F, G**). Contrastingly, PBS treated networks had more stable fluctuations in bursts during recordings. These networks maintained the trend with most occurrences of burst having <= 10 spikes, and not exceeding 20 spikes per burst by the 2nd phase recording (**Figure 7H-J**), unlike the inhibited networks, which had up to 1000 spikes per burst during the 2nd phase recording (**Figure 7F**).

Further investigation revealed that for the inhibited networks, the mean ISI in network bursts decreased from 24.0ms at baseline to 9.6ms during the 1st phase recording and increased slightly during the 2nd phase recording (13.9ms) and 3rd phase (17.3ms) (**Figure 8A-C**). The changes in ISI in bursts were significant for all inhibited networks ($p < 0.01$). The PBS treated networks also experienced some changes in the ISI in burst decreasing from 28.2ms at baseline to 25.6ms during the 1st phase recording and fluctuating between 29.7ms and 20.8ms at 2nd and 3rd phases respectively (**Figure 8D-F**). These changes were not found to be significant. Looking at network recovery, we also found that for all the inhibited networks, there were significant increases in the mean and median ISI within bursts at 12hrs and 24hrs post treatment ($p < 0.0001$) compared to baseline recordings (**Figure 9A, B**). No significant changes were found for the control or PBS treated networks.

We also found that burst duration at 12 and 24hrs recovery recordings was significantly longer than burst duration at baseline ($p = <0.0001$) for the inhibited networks (**Figure 9 C, D**). There seemed to be a significant difference in burst duration between baseline and 3rd phase recording ($p = 0.009$), and between 2nd and 3rd phase recording ($p = 0.009$) for the control network. Also, one PBS treated network appeared to have significant changes in burst duration between baseline and 1st, 2^{nd,} and 3rd phase recording ($p = 0.0003$; $p = 0.0003$; $p = 0.003$ respectively). Finally, we also found that at baseline, the control network had 72% of spikes located in network bursts, while PBS treated networks had 52% and 77% of spikes in network bursts (**Figure 9E**). This decreased drastically by 1st phase recording and remained at <40% for all subsequent recordings. On the other hand, the inhibited networks showed an opposite trend, where baseline activity had <40% spikes located in network bursts, increasing to approximately 80% by 3rd phase recording. All DCZ treated networks had a decrease in activity at 2hrs recovery recording (<40% of spikes located in network bursts). Activity increased at 12hrs with up to 95% of spikes located in network bursts, and up to 98% spikes in network bursts by 24hrs recovery recording.

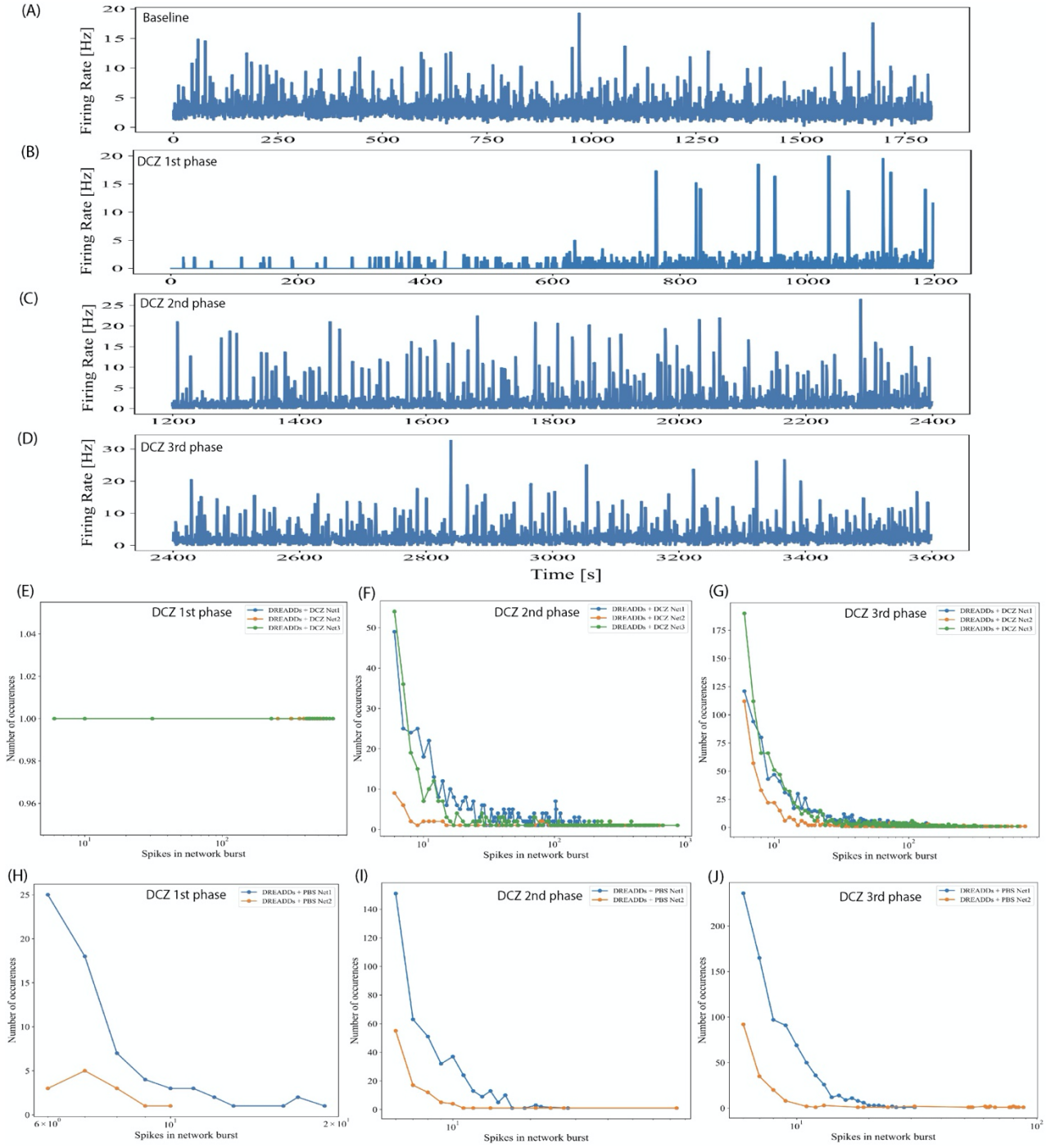

Figure 7. Neural network activity at baseline and in response to DREADDs-mediated inhibition of excitatory synaptic transmission. Each panel **(A-D)** show a trace generated from 64 recording channels of spontaneous activity of one DCZ treated network at 28DIV. **(A)** show the spontaneous firing rate at baseline, **(B)** the first 20 minutes recording of spontaneous activity during DCZ treatment, **(C)** the second 20 minutes recording of spontaneous activity during DCZ treatment and **(D)** the third 20 minutes recording of spontaneous activity during DCZ treatment. The x-axis denotes time in seconds and the y-axis denotes firing rate in Hz. The spikes in burst (x-axis) and number of occurrences (y-axis) for 1st, 2nd, and 3rd phase recordings is shown for DCZ treated networks **(E-G)** and for PBS vehicle networks **(H-J)**.

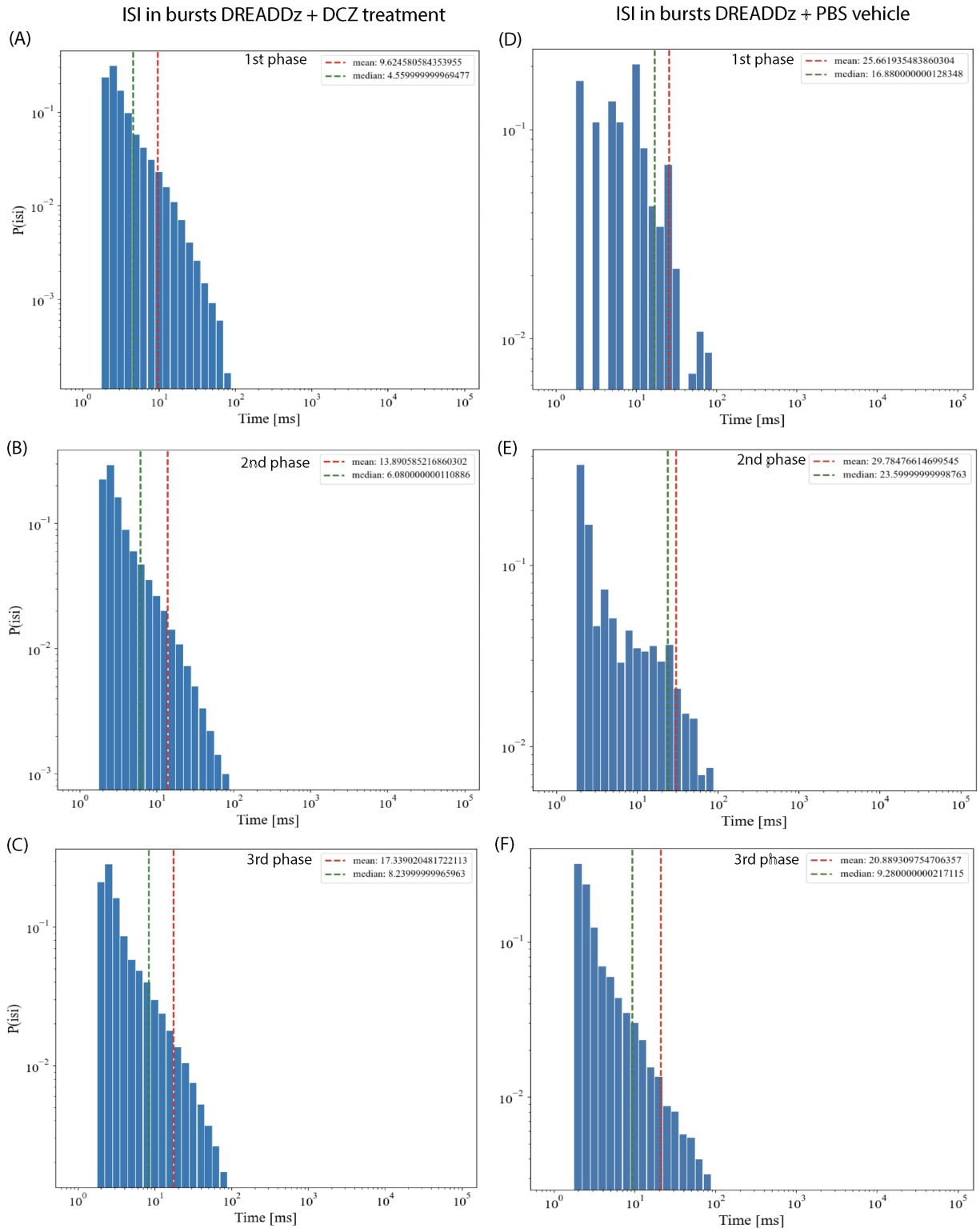

Figure 8. Histograms of interspike intervals of spikes in burst during DCZ treatment and PBS vehicle 1st, 2nd, and 3rd phase recordings. The green stippled line indicates the median ISI in milliseconds and the red stippled line indicates the mean ISI in milliseconds. The x-axis denotes time (ms) and the y-axis denotes the probability P(ISI).

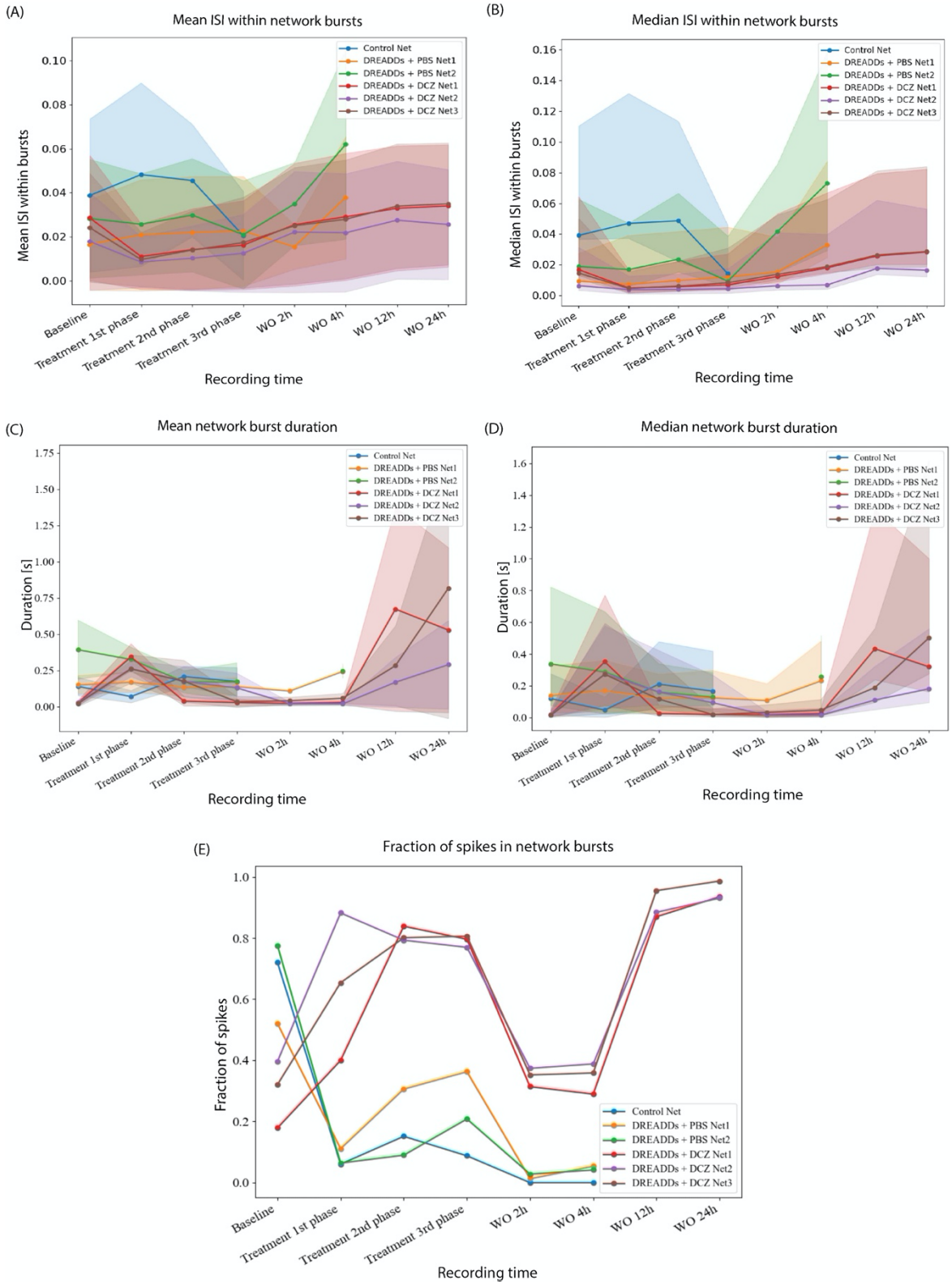

Figure 9. Neural network activity and burst characteristics at baseline, treatment, and recovery for all networks at 28 DIV. **(A)** Line graph showing the mean ISI within bursts (y-axis) across recording session (x-axis), with the mean ± standard deviation of the mean depicted as the shaded area. **(B)** Line graph showing the median ISI within burst (y-axis) across recording session (x-axis), with the median ± median absolute deviation depicted as the shaded area. Line graphs showing the mean **(C)** and median **(D)** network burst duration in seconds (y-axis) across recording session (x-axis). (E) Line graph showing the fraction of spikes in network bursts (y-axis) for each recording session (x-axis).

4 Discussion

Cortical neurons in vitro formed densely connected networks on the MEAs by 7 DIV as seen in **Figure 1**, and by 14 DIV, neurons had distinct structural organization with prominent axon fasciculation, and dendritic connections across the entire network, as well as mature excitatory and inhibitory receptors as seen in **Figure 3**. Functional interactions between maturing excitatory and inhibitory synapses result in dynamic spiking activity and the emergence of network bursts (Teppola et al., 2019). Increasing either excitation or inhibition can therefore be expected to result in aberrant bursting dynamics in neural networks, thus we set out to investigate how bursting dynamics are affected when excitatory synaptic transmission is inhibited. To do this, we took advantage of the unique opportunity that DREADDs provide to selectively target excitatory activity, and after transducing the networks with AAV 2/1 hM4Di CaMKlla-DREADDs, we proceeded to activate the DREADDs with DCZ at 14 DIV, 21 DIV and 28 DIV. Our primary findings are: (1) inhibition of excitatory synaptic transmission results in an increase in the occurrences of bursts, and more bursts with >100 spikes per burst in inhibited networks; (2) Inhibited networks recovered activity in the presence of DCZ indicating rapid homeostatic response to network silencing; (3) Inhibited networks maintained high levels of synchrony at 24hrs recovery with up to 98% of spikes located in network bursts.

Network activity and bursting dynamics are inherently unique to each network in vitro, nonetheless, in our study all networks exhibited some degree of network bursting activity by 14 DIV with most bursts having between 5 – 10 spikes, and rarer instances of bursts of larger number of spikes. Early network bursts are significant for network development and maturity and are deemed to be physiologically relevant for neural information processing and synaptic plasticity (Lisman, 1997). In developing networks, bursts act as more reliable determinants of neurotransmitter release than single spikes (Lisman, 1997, Delattre et al., 2015), thus synaptic efficacy and facilitation rely on network bursts to increase the probability of postsynaptic response to presynaptic inputs. While others (Marom and Shahaf, 2002, Wagenaar et al., 2006, Chiappalone et al., 2006, Bisio et al., 2014) reported overall increase in network bursts at mature stages in vitro (21 – 28 DIV), our inhibited networks exhibited patterns of high frequency network bursts which occurred in short, defined trains, with increasingly greater number of spikes as shown in **Figure 6**. Due to the high frequency, these bursts appeared to be akin to 'superbursts' typically observed at earlier development, before the network establishes more mature neuronal phenotypes (Stephens et al., 2012) and before GABA receptors mature. Furthermore, as it was found that > 95% of all spikes were in network bursts in the inhibited networks, we can speculate that all active neurons participated in the network burst, and this could possibly mean that there was very little inhibition in the network.

While there may be different explanations as to the cause of this increased global activation and decreased inhibition, the most plausible one is linked to our experimental set up and methods used. In our study, the activation of hM4Di DREADDs blocks cAMP production (by Gai protein blockade of adenylate cyclase), which results in neurons being unable to detect and respond to extracellular signals. Thus, DREADDs expression and activation on excitatory neurons likely prevents neurons from reliably responding to excitatory post synaptic potentials, thereby causing disruption in activity, and the potential development of inhibitory synapses. It is well documented that excitatory

synaptic activity regulates the development and maintenance of inhibitory synapses on excitatory neurons (Lin et al., 2008), and that deprivation of excitatory synaptic activity reduces the density of synaptic GABA receptors, and the number of functional inhibitory synapses in cortical cultures (Kilman et al., 2002) and hippocampal slices (Ramakers et al., 1994, Muramoto et al., 1996, Chub and O'Donovan, 1998). In our study, the consequence of excitatory synaptic inhibition at 14DIV was a subsequent increase in burst frequency and the frequency of bursts with >100 spikes / burst, indicating impaired inhibitory synaptic development and overall, less inhibition in the network.

Although the emerging picture is that E/I synaptic activity is the single most important factor regulating neural network bursting behaviour, our results also indicate that there are intrinsic homeostatic mechanisms at work. According to the theory of homeostatic plasticity, network activity is stabilized by a negative feedback process where a forceful change in activity is resisted, and the system returns to a tolerated dynamic range (Turrigiano, 1999). The data presented in our study show that inhibited networks were able to recover network bursts during DCZ exposure, supporting several previous studies where networks bursts were maintained in the presence of activity suppressing chemogens (Chub and O'Donovan, 1998, Li et al., 2007, Zeldenrust et al., 2018). The exact mechanism for recovery during chemogenetic manipulation is unknown, however, we posit that several homeostatic factors including alterations in neuromodulator levels and neurotransmitter release (Ramakers et al., 1994, Muramoto et al., 1996, Chub and O'Donovan, 1998) or sensitivity (Turrigiano et al., 1998, Desai et al., 1999) contributed to the network rescuing spontaneous activity. The presence of 95% spikes in network bursts 12hrs post removal of the DCZ suggests that silencing excitatory synaptic transmission may have lowered the spike threshold of excitatory neurons causing neurons to respond more robustly to activation during network recovery. However, as this activity was maintained for up to 24hrs, there must exist multiple mechanisms regulating the sensitivity of neurons to inputs while also managing possible excitotoxic cell death up to 28DIV. This raises an interesting question of how these different regulatory mechanisms are balanced.

As the networks appeared to not have survived past 30 DIV, the long-term implications that excitatory synaptic silencing have on functional connectivity is unknown. However, there might have been some remodeling of synaptic attributes and/or reorganization of the structural network, which would make the network less efficient at information transmission due to increased noise in the network. This hypothesis can be tested further using high density MEAs that offer higher spatial resolution for network connectivity investigation.

5 Data availability statement

The raw data that support the findings of this study will be made available by the authors.

6 Conflict of Interest

The authors declare that the research was conducted in the absence of any commercial or financial relationships that could be construed as a potential conflict of interest.

7 Author Contributions

This study was conceived and designed by JSW, AS and IS. All data collection was done by JSW who also drafted the manuscript. NC performed all data analysis and statistical analysis. AS and IS helped with the manuscript revision process, and all authors have read and approved the final version of the manuscript.

8 Funding

This project is part of the SOCRATES (Self-Organizing Computational Substrates) project and is funded by The Research Council of Norway (NFR, IKT Pluss), Grant number: 270961.

9 Acknowledgments

The authors would like to thank Prof. Morten Høydal, Department of Circulation and Medical Imaging, NTNU, for facilitating access to the Axion electrophysiology system, and Dr. Rajeevkumar Nair Raveendran, Viral Core Facility, Kavli Institute for Systems Neurocience, NTNU, for the design and preparation of the DREADDs constructs.

10 References

ALEXANDER, G. M., ROGAN, S. C., ABBAS, A. I., ARMBRUSTER, B. N., PEI, Y., ALLEN, J. A., NONNEMAN, R. J., HARTMANN, J., MOY, S. S., NICOLELIS, M. A., MCNAMARA, J. O. & ROTH, B. L. 2009. Remote Control of Neuronal Activity in Transgenic Mice Expressing Evolved G Protein-Coupled Receptors. *Neuron,* 63**,** 27-39.

ARMBRUSTER, B. N., LI, X., PAUSCH, M. H., HERLITZE, S. & ROTH, B. L. 2007. Evolving the lock to fit the key to create a family of G protein-coupled receptors potently activated by an inert ligand. *Proceedings of the National Academy of Sciences,* 104**,** 5163-5168.

BAKKUM, D. J., RADIVOJEVIC, M., FREY, U., FRANKE, F., HIERLEMANN, A. & TAKAHASHI, H. 2013. Parameters for burst detection. *Front Comput Neurosci,* 7**,** 193.

BALTZ, T., DE LIMA, A. & VOIGT, T. 2010. Contribution of GABAergic interneurons to the development of spontaneous activity patterns in cultured neocortical networks. *Frontiers in Cellular Neuroscience,* 4.

BEN-ARI, Y. 2001. Developing networks play a similar melody. *Trends Neurosci,* 24**,** 353-60.

BISIO, M., BOSCA, A., PASQUALE, V., BERDONDINI, L. & CHIAPPALONE, M. 2014. Emergence of bursting activity in connected neuronal sub-populations. *PLoS One,* 9**,** e107400.

BJORKLI, C., EBBESEN, N. C., JULIAN, J. B., WITTER, M. P., SANDVIG, A. & SANDVIG, I. 2022. Manipulation of neuronal activity in the entorhinal-hippocampal circuit affects intraneuronal amyloid-β levels. *bioRxiv***,** 2022.07.05.498797.

BLANKENSHIP, A. G. & FELLER, M. B. 2010. Mechanisms underlying spontaneous patterned activity in developing neural circuits. *Nat Rev Neurosci,* 11**,** 18-29.

BURGARD, E. C. & HABLITZ, J. J. 1994. Developmental-Changes in the Voltage-Dependence of Neocortical Nmda Responses. *Developmental Brain Research,* 80**,** 275-278.

CHIAPPALONE, M., BOVE, M., VATO, A., TEDESCO, M. & MARTINOIA, S. 2006. Dissociated cortical networks show spontaneously correlated activity patterns during in vitro development. *Brain Res,* 1093**,** 41-53.

CHIAPPALONE, M., VATO, A., BERDONDINI, L., KOUDELKA-HEP, M. & MARTINOIA, S. 2007. Network dynamics and synchronous activity in cultured cortical neurons. *Int J Neural Syst,* 17**,** 87-103.

CHIU, C. & WELIKY, M. 2001. Spontaneous activity in developing ferret visual cortex in vivo. *J Neurosci,* 21**,** 8906-14.

CHUB, N. & O'DONOVAN, M. J. 1998. Blockade and recovery of spontaneous rhythmic activity after application of neurotransmitter antagonists to spinal networks of the chick embryo. *J Neurosci,* 18**,** 294-306.

DARBON, P., YVON, C., LEGRAND, J. C. & STREIT, J. 2004. INaP underlies intrinsic spiking and rhythm generation in networks of cultured rat spinal cord neurons. *Eur J Neurosci,* 20**,** 976-88.

DELATTRE, V., KELLER, D., PERICH, M., MARKRAM, H. & MULLER, E. B. 2015. Network-timing-dependent plasticity. *Frontiers in cellular neuroscience,* 9**,** 220-220.

DESAI, N. S., RUTHERFORD, L. C. & TURRIGIANO, G. G. 1999. Plasticity in the intrinsic excitability of cortical pyramidal neurons. *Nat Neurosci,* 2**,** 515-20.

DIZON, M. J. & KHODAKHAH, K. 2011. The role of interneurons in shaping Purkinje cell responses in the cerebellar cortex. *J Neurosci,* 31**,** 10463-73.

438 FARDET, T., BALLANDRAS, M., BOTTANI, S., METENS, S. & MONCEAU, P. 2018. Understanding the
439 Generation of Network Bursts by Adaptive Oscillatory Neurons. *Front Neurosci,* 12**,** 41.

440 GANDOLFO, M., MACCIONE, A., TEDESCO, M., MARTINOIA, S. & BERDONDINI, L. 2010. Tracking
441 burst patterns in hippocampal cultures with high-density CMOS-MEAs. *J Neural Eng,* 7**,** 056001.

442 HAARANEN, M., SCHAFER, A., JARVI, V. & HYYTIA, P. 2020a. Chemogenetic Stimulation and
443 Silencing of the Insula, Amygdala, Nucleus Accumbens, and Their Connections Differentially
444 Modulate Alcohol Drinking in Rats. *Frontiers in Behavioral Neuroscience,* 14.

445 HAARANEN, M., SCUPPA, G., TAMBALO, S., JARVI, V., BERTOZZI, S. M., ARMIROTTI, A.,
446 SOMMER, W. H., BIFONE, A. & HYYTIA, P. 2020b. Anterior insula stimulation suppresses
447 appetitive behavior while inducing forebrain activation in alcohol-preferring rats. *Translational*
448 *Psychiatry,* 10.

449 HOEHNE, A., MCFADDEN, M. H. & DIGREGORIO, D. A. 2020. Feed-forward recruitment of electrical
450 synapses enhances synchronous spiking in the mouse cerebellar cortex. *Elife,* 9.

451 KAMIOKA, H., MAEDA, E., JIMBO, Y., ROBINSON, H. P. & KAWANA, A. 1996. Spontaneous periodic
452 synchronized bursting during formation of mature patterns of connections in cortical cultures.
453 *Neurosci Lett,* 206**,** 109-12.

454 KHAMBHATI, A. N. & BASSETT, D. S. 2016. A Powerful DREADD: Revealing Structural Drivers of
455 Functional Dynamics. *Neuron,* 91**,** 213-5.

456 KILMAN, V., VAN ROSSUM, M. C. W. & TURRIGIANO, G. G. 2002. Activity Deprivation Reduces
457 Miniature IPSC Amplitude by Decreasing the Number of Postsynaptic
458 GABA_A Receptors Clustered at Neocortical Synapses. *The Journal of*
459 *Neuroscience,* 22**,** 1328.

460 KUDELA, P., FRANASZCZUK, P. J. & BERGEY, G. K. 2003. Changing excitation and inhibition in
461 simulated neural networks: effects on induced bursting behavior. *Biol Cybern,* 88**,** 276-85.

462 LEBONVILLE, C. L., PANICCIA, J. E., PAREKH, S. V., WANGLER, L. M., JONES, M. E., FUCHS, R. A.
463 & LYSLE, D. T. 2020. Expression of a heroin contextually conditioned immune effect in male rats
464 requires CaMKIIα-expressing neurons in dorsal, but not ventral, subiculum and hippocampal CA1.
465 *Brain, Behavior, and Immunity,* 89**,** 414-422.

466 LI, X., ZHOU, W., ZENG, S., LIU, M. & LUO, Q. 2007. Long-term recording on multi-electrode array
467 reveals degraded inhibitory connection in neuronal network development. *Biosens Bioelectron,* 22**,**
468 1538-43.

469 LIN, Y., BLOODGOOD, B. L., HAUSER, J. L., LAPAN, A. D., KOON, A. C., KIM, T. K., HU, L. S.,
470 MALIK, A. N. & GREENBERG, M. E. 2008. Activity-dependent regulation of inhibitory synapse
471 development by Npas4. *Nature,* 455**,** 1198-204.

472 LISMAN, J. E. 1997. Bursts as a unit of neural information: making unreliable synapses reliable. *Trends*
473 *Neurosci,* 20**,** 38-43.

474 MAGALHAES, K. S., DA SILVA, M. P., MECAWI, A. S., PATON, J. F. R., MACHADO, B. H. &
475 MORAES, D. J. A. 2021. Intrinsic and synaptic mechanisms controlling the expiratory activity of
476 excitatory lateral parafacial neurones of rats. *J Physiol,* 599**,** 4925-4948.

477 MAROM, S. & SHAHAF, G. 2002. Development, learning and memory in large random networks of cortical
478 neurons: lessons beyond anatomy. *Q Rev Biophys,* 35**,** 63-87.

479 MURAMOTO, T., MENDELSON, B., PHELAN, K. D., GARCIA-RILL, E., SKINNER, R. D. &
480 PUSKARICH-MAY, C. 1996. Developmental changes in the effects of serotonin and N-methyl-D-
481 aspartate on intrinsic membrane properties of embryonic chick motoneurons. *Neuroscience,* 75**,** 607-
482 18.

NAGAI, Y., MIYAKAWA, N., TAKUWA, H., HORI, Y., OYAMA, K., JI, B., TAKAHASHI, M., HUANG, X. P., SLOCUM, S. T., DIBERTO, J. F., XIONG, Y., URUSHIHATA, T., HIRABAYASHI, T., FUJIMOTO, A., MIMURA, K., ENGLISH, J. G., LIU, J., INOUE, K. I., KUMATA, K., SEKI, C., ONO, M., SHIMOJO, M., ZHANG, M. R., TOMITA, Y., NAKAHARA, J., SUHARA, T., TAKADA, M., HIGUCHI, M., JIN, J., ROTH, B. L. & MINAMIMOTO, T. 2020. Deschloroclozapine, a potent and selective chemogenetic actuator enables rapid neuronal and behavioral modulations in mice and monkeys. *Nat Neurosci,* 23**,** 1157-1167.

OBIEN, M. E. J., DELIGKARIS, K., BULLMANN, T., BAKKUM, D. J. & FREY, U. 2015. Revealing neuronal function through microelectrode array recordings. *Frontiers in Neuroscience,* 8.

OPITZ, T., DE LIMA, A. D. & VOIGT, T. 2002. Spontaneous development of synchronous oscillatory activity during maturation of cortical networks in vitro. *Journal of neurophysiology,* 88**,** 2196-2206.

OZAWA, A. & ARAKAWA, H. 2021. Chemogenetics drives paradigm change in the investigation of behavioral circuits and neural mechanisms underlying drug action. *Behav Brain Res,* 406**,** 113234.

PANTHI, S. & LEITCH, B. 2019. The impact of silencing feed-forward parvalbumin-expressing inhibitory interneurons in the cortico-thalamocortical network on seizure generation and behaviour. *Neurobiol Dis,* 132**,** 104610.

PENA, F. & RAMIREZ, J. M. 2004. Substance P-mediated modulation of pacemaker properties in the mammalian respiratory network. *J Neurosci,* 24**,** 7549-56.

RAMAKERS, G. J., CORNER, M. A. & HABETS, A. M. 1990. Development in the absence of spontaneous bioelectric activity results in increased stereotyped burst firing in cultures of dissociated cerebral cortex. *Exp Brain Res,* 79**,** 157-66.

RAMAKERS, G. J., VAN GALEN, H., FEENSTRA, M. G., CORNER, M. A. & BOER, G. J. 1994. Activity-dependent plasticity of inhibitory and excitatory amino acid transmitter systems in cultured rat cerebral cortex. *Int J Dev Neurosci,* 12**,** 611-21.

RAUS BALIND, S., MAGÓ, Á., AHMADI, M., KIS, N., VARGA-NÉMETH, Z., LŐRINCZ, A. & MAKARA, J. K. 2019. Diverse synaptic and dendritic mechanisms of complex spike burst generation in hippocampal CA3 pyramidal cells. *Nature Communications,* 10**,** 1859.

ROBINSON, H. P., KAWAHARA, M., JIMBO, Y., TORIMITSU, K., KURODA, Y. & KAWANA, A. 1993. Periodic synchronized bursting and intracellular calcium transients elicited by low magnesium in cultured cortical neurons. *J Neurophysiol,* 70**,** 1606-16.

SCHROETER, M. S., CHARLESWORTH, P., KITZBICHLER, M. G., PAULSEN, O. & BULLMORE, E. T. 2015. Emergence of rich-club topology and coordinated dynamics in development of hippocampal functional networks in vitro. *J Neurosci,* 35**,** 5459-70.

STEPHENS, C. L., TODA, H., PALMER, T. D., DEMARSE, T. B. & ORMEROD, B. K. 2012. Adult neural progenitor cells reactivate superbursting in mature neural networks. *Exp Neurol,* 234**,** 20-30.

SUN, J. J., KILB, W. & LUHMANN, H. J. 2010. Self-organization of repetitive spike patterns in developing neuronal networks in vitro. *Eur J Neurosci,* 32**,** 1289-99.

SURESH, J., RADOJICIC, M., PESCE, L. L., BHANSALI, A., WANG, J., TRYBA, A. K., MARKS, J. D. & VAN DRONGELEN, W. 2016. Network burst activity in hippocampal neuronal cultures: the role of synaptic and intrinsic currents. *J Neurophysiol,* 115**,** 3073-89.

TEPPOLA, H., ACIMOVIC, J. & LINNE, M. L. 2019. Unique Features of Network Bursts Emerge From the Complex Interplay of Excitatory and Inhibitory Receptors in Rat Neocortical Networks. *Frontiers in Cellular Neuroscience,* 13.

TURRIGIANO, G. G. 1999. Homeostatic plasticity in neuronal networks: the more things change, the more they stay the same. *Trends Neurosci,* 22**,** 221-7.

528 TURRIGIANO, G. G., LESLIE, K. R., DESAI, N. S., RUTHERFORD, L. C. & NELSON, S. B. 1998.
529 Activity-dependent scaling of quantal amplitude in neocortical neurons. *Nature,* 391**,** 892-6.

530 URBAN, D. J. & ROTH, B. L. 2015. DREADDs (designer receptors exclusively activated by designer drugs):
531 chemogenetic tools with therapeutic utility. *Annu Rev Pharmacol Toxicol,* 55**,** 399-417.

532 VAN DRONGELEN, W., KOCH, H., ELSEN, F. P., LEE, H. C., MREJERU, A., DOREN, E.,
533 MARCUCCILLI, C. J., HERELD, M., STEVENS, R. L. & RAMIREZ, J. M. 2006. Role of persistent
534 sodium current in bursting activity of mouse neocortical networks in vitro. *J Neurophysiol,* 96**,** 2564-
535 77.

536 WAGENAAR, D. A., PINE, J. & POTTER, S. M. 2006. An extremely rich repertoire of bursting patterns
537 during the development of cortical cultures. *BMC Neurosci,* 7**,** 11.

538 WHISSELL, P. D., TOHYAMA, S. & MARTIN, L. J. 2016. The Use of DREADDs to Deconstruct Behavior.
539 *Front Genet,* 7**,** 70.

540 ZELDENRUST, F., WADMAN, W. J. & ENGLITZ, B. 2018. Neural Coding With Bursts-Current State and
541 Future Perspectives. *Frontiers in computational neuroscience,* 12**,** 48-48.

542